TITLE:

Semiquantum molecular dynamics simulation of liquid water by time-dependent Hartree approach.

AUTHOR(S):

Kim, Hyeon-Deuk; Ando, Koji

CITATION:

Kim, Hyeon-Deuk ...[et al]. Semiquantum molecular dynamics simulation of liquid water by time-dependent Hartree approach.. The Journal of chemical physics 2009, 131(6): 064501.

ISSUE DATE:

2009-08-14

URL:

http://hdl.handle.net/2433/91543

RIGHT:

© 2009 American Institute of Physics

京都大学学術情報リポジトリ
KURENAI 紅
Kyoto University Research Information Repository

京都大学 KYOTO UNIVERSITY
A Self-archived copy in
Kyoto University Research Information Repository
https://repository.kulib.kyoto-u.ac.jp
京都大学学術情報リポジトリ KURENAI 紅 Kyoto University Research Information Repository

THE JOURNAL OF CHEMICAL PHYSICS **131**, 064501 (2009)

Semiquantum molecular dynamics simulation of liquid water by time-dependent Hartree approach

Kim Hyeon-Deuk[a] and Koji Ando
Department of Chemistry, Kyoto University, Kyoto 606-8502, Japan

(Received 29 May 2009; accepted 16 July 2009; published online 10 August 2009)

Semiquantum liquid water molecular dynamics simulation was developed using the time-dependent Hartree approach. The classical intra- and intermolecular potential functions of water were extended to describe the wave packet (WP) hydrogen atoms. The equations of motion with an extended phase space including auxiliary coordinates and momenta representing the hydrogen WP widths were derived and solved. The molecular dynamics simulation of semiquantum water demonstrated that the semiquantum hydrogen atoms make the liquid water less structured and the hydrogen bonds weakened. The poor structurization in liquid water was inferred from the increased mobility of a water molecule and the redshift of OH stretching frequency. The zero-point energy introduced by the semiquantum hydrogens enhances the anharmonic potential effects and contributes to the redshifted OH stretching vibration. We found a significant peak around 4400 cm^{-1} in the absorption spectrum resulting from the energy exchange between the WP width dynamics and the coupling of the OH stretching mode and the rotational motion of each water. We proposed that a liquid free energy landscape is smoothed due to semiquantum hydrogen atoms, and influences the liquid structure and dynamics. © *2009 American Institute of Physics*. [DOI: 10.1063/1.3200937]

I. INTRODUCTION

The many body dynamics of chemical reactions are typically too complicated for a fully quantum-mechanical analysis. Although considerable progress has been made in the development of exact quantum-mechanical methods,[1,2] they are still only applicable to relatively small molecular systems and simple models. In contrast, classical dynamics methods are routinely used to study complex chemical problems involving many thousands of particles. It is a fact that, however, quantum effects such as zero-point energy (ZPE), tunneling, dephasing, interference, branching, etc., are essential in chemistry. The ZPE of a proton, about 4 kcal/mol, implies that the quantum nature is far from negligible. This affects the structure and dynamics in ways beyond the classical mechanical description. One is, therefore, necessarily interested in approaches that capture the quantum phenomena in many degrees of freedom. A number of such approaches involving semiclassical and mixed quantum-classical dynamics have been proposed and applied in recent years, and remain under active development.

The anomalous properties of liquid water and its role in chemistry and biology have made it a subject of intense research.[3–5] On the computational side, the earliest atomistic simulations of the ambient liquid using a simple empirical potential have been performed for many decades. Many improved potentials have been developed and shown to provide better agreement with experiments when used in classical molecular dynamics (MD) and Monte Carlo simulations.[6–13] Classical mechanical MD is nowadays very straightforward once the force field parameters are decided, only depending on the quality of the force field and the sufficiency of the statistical sampling of the trajectories.

The first quantum-mechanical simulations of the static equilibrium properties of the liquid were performed, when the path-integral Monte Carlo (PIMC) method was used to assess the effect of quantum-mechanical fluctuations on the liquid structure.[14,15] However, the role of quantum-mechanical effects in the dynamics of the liquid have been investigated quite recently. The centroid molecular dynamics (CMD) method to study the dynamics of a flexible simple point-charge (SPC/Fd) model of ambient water was proposed, and modeled para-hydrogen and ortho-deuterium.[16–18] Several CMD studies of the orientational and translational motions in a rigid-body (TIP4) water model have appeared.[19,20] The dynamics of a flexible water model was also studied using the Feynman–Kleinert linearized path-integral approach,[21] while the ring-polymer MD method was focused on a rigid water model.[22] All such semiquantum studies concluded that quantum-mechanical fluctuations tend to enhance the diffusion in the ambient liquid, the calculated increase in the self-diffusion coefficient over that obtained in a purely classical simulation. This increase in the diffusion coefficient is consistent with the decrease in the structure of the liquid due to quantum-mechanical effects that was observed in the earlier PIMC calculations.[14–16,18]

The primary motivation of this work is to devise a practical and efficient simulation method to take account of the nuclear quantum aspects in the liquid water dynamics and structure. We thus develop the semiquantum water (SQW) MD simulation using the semiquantum time-dependent Hartree (SQTDH) theory proposed recently.[23,24] The SQTDH is based on the time-dependent variational principle with a re-

[a]Electronic mail: kim@kuchem.kyoto-u.ac.jp.

 © 2009 American Institute of Physics

Downloaded 14 Sep 2009 to 171.64.125.187. Redistribution subject to AIP license or copyright; see http://jcp.aip.org/jcp/copyright.jsp

京都大学 KYOTO UNIVERSITY
A Self-archived copy in
Kyoto University Research Information Repository
https://repository.kulib.kyoto-u.ac.jp
京都大学学術情報リポジトリ KURENAI 紅 Kyoto University Research Information Repository

striction of the Hilbert space to a subspace of the squeezed coherent state wave packet (WP), which yields the equations of motion (EOMs) with an extended phase space including auxiliary coordinates and momenta representing the WP widths. The EOMs in SQTDH are quite similar to the classical EOM, and many of the standard numerical tools of classical MD can be applied to them, facilitating its implementation and applications. Approximate accounts of the WP delocalizing and the ZPE effects are expected to offer insights beyond the current understanding from classical simulations. Indeed, proton delocalization phenomena were experimentally observed in water systems.[25,26]

The delocalized nature of quantum particles would be well captured by semiclassical WP approaches, from the primitive version of the Gaussian WP method[27,28] to the recent sophistication and complication of, e.g., multiconfiguration time-dependent Hartree[29–31] and multiple spawning[32,33] approaches. However, application of the Gaussian WP method to condensed phase MD simulations is rather scarce, presumably due to the high computational cost for the fully correlated WP or the lack of an obvious adequate factorization scheme. It is also interesting to note that the fourth-order expansion in SQTHD is essentially equivalent to the second-order quantized Hamiltonian dynamics (QHD-2) theory derived via an apparently different route from mixed quantum-classical Heisenberg EOM,[34–36] and to the quantal cumulant dynamics method.[37]

Our paper is organized as follows. In Secs. II and III, we introduce the three-dimensional (3D) SQTDH for a many body system, and develop the 3D SQW MD simulation, respectively. The potential functions for the full-classical water (FCW) MD simulation are extended to the potentials describing SQW there. The details of our SQW and FCW MD simulations are explained in Sec. IV. The calculated results for SQW are directly compared to those for FCW, and the important roles of the semiquantum hydrogen atoms are discussed in Sec. V. Section VI gives the concluding remarks.

II. THREE-DIMENSIONAL SEMIQUANTUM TIME-DEPENDENT HARTREE APPROACH FOR A MANY BODY SYSTEM

The 3D SQTDH for a many body (N-particles) system which can be applied to the 3D SQW MD simulation is explained here. For simplicity, $\hbar=1$ and all the coordinates are mass scaled. We invoke the 3D time-dependent Hartree approximation with the N-independent 3D squeezed coherent state Gaussian WP basis functions,

$$\Psi(\{x_i,y_i,z_i\},t)=\prod_{i=1}^{N}\Psi_i(x_i,y_i,z_i,t), \tag{1}$$

where

$$\begin{aligned}\Psi_i(x_i,y_i,z_i,t)=N_{x_i}N_{y_i}N_{z_i}\exp[&A_{x_i}(t)\{x_i-q_{x_i}(t)\}^2+ip_{x_i}(t)\\&\times\{x_i-q_{x_i}(t)\}]\exp[A_{y_i}(t)\{y_i-q_{y_i}(t)\}^2\\&+ip_{y_i}(t)\{y_i-q_{y_i}(t)\}]\exp[A_{z_i}(t)\{z_i-q_{z_i}(t)\}^2\\&+ip_{z_i}(t)\{z_i-q_{z_i}(t)\}].\end{aligned} \tag{2}$$

A_{α_i} with $\alpha_i=x_i,y_i$ or z_i is introduced as

$$A_{\alpha_i}(t)=\frac{-1+2i\rho_{\alpha_i}(t)\Lambda_{\alpha_i}(t)}{4\rho_{\alpha_i}^2(t)}, \tag{3}$$

where $\rho_{\alpha_i}(t)$ and $\Lambda_{\alpha_i}(t)$ correspond to WP width and its momentum, respectively. The other important factor $N_{\alpha_i}=(2\pi\rho_{\alpha_i}^2(t))^{-1/4}$ is a normalization factor. The WP function (2) is completely specified by the time-dependent parameters $\{q_{\alpha_i}(t),p_{\alpha_i}(t),\rho_{\alpha_i}(t),\Lambda_{\alpha_i}(t)\}$ to be determined through the following time-dependent variational principle.

The action integral is defined as

$$\Gamma\equiv\int Ldt=\int dt\langle\Psi,t|i\frac{\partial}{\partial t}-\hat{H}|\Psi,t\rangle, \tag{4}$$

with the Lagrangian L. The Hamiltonian operator $\hat{H}$ is given by

$$\hat{H}=\sum_{i=1}^{N}-\frac{1}{2}\left[\frac{\partial^2}{\partial x_i^2}+\frac{\partial^2}{\partial y_i^2}+\frac{\partial^2}{\partial z_i^2}\right]+\sum_{i<j}^{N}V_{ij}(x_{ij},y_{ij},z_{ij}), \tag{5}$$

where $x_{ij}=x_i-x_j$, $y_{ij}=y_i-y_j$, and $z_{ij}=z_i-z_j$. Equation (4) with Eqs. (2) and (5) leads to

$$\begin{aligned}L=\sum_{i=1}^{N}\Bigg[&p_{x_i}\dot{q}_{x_i}+p_{y_i}\dot{q}_{y_i}+p_{z_i}\dot{q}_{z_i}+\frac{1}{2}(\Lambda_{x_i}\dot{\rho}_{x_i}+\Lambda_{y_i}\dot{\rho}_{y_i}+\Lambda_{z_i}\dot{\rho}_{z_i})\\&-\frac{1}{2}(\dot{\Lambda}_{x_i}\rho_{x_i}+\dot{\Lambda}_{y_i}\rho_{y_i}+\dot{\Lambda}_{z_i}\rho_{z_i})-\frac{1}{2}(p_{x_i}^2+p_{y_i}^2+p_{z_i}^2)\\&-\frac{1}{2}(\Lambda_{x_i}^2+\Lambda_{y_i}^2+\Lambda_{z_i}^2)-\frac{1}{8}(\rho_{x_i}^{-2}+\rho_{y_i}^{-2}+\rho_{z_i}^{-2})\Bigg]\\&-\sum_{i<j}^{N}\langle V_{ij}(x_{ij},y_{ij},z_{ij})\rangle.\end{aligned} \tag{6}$$

Here, the potential expectation $\langle V_{ij}(x_{ij},y_{ij},z_{ij})\rangle$ is a function of $\{q_{\alpha_i},\rho_{\alpha_i}\}$. Finally, the time-dependent variational principle, $\delta\Gamma/\delta q_{\alpha_i}=0$, etc., results in the EOM,

$$\begin{aligned}\dot{q}_{\alpha_i}&=\frac{\partial H_{\text{ext}}}{\partial p_{\alpha_i}},\quad \dot{p}_{\alpha_i}=-\frac{\partial H_{\text{ext}}}{\partial q_{\alpha_i}},\\ \dot{\rho}_{\alpha_i}&=\frac{\partial H_{\text{ext}}}{\partial \Lambda_{\alpha_i}},\quad \dot{\Lambda}_{\alpha_i}=-\frac{\partial H_{\text{ext}}}{\partial \rho_{\alpha_i}},\end{aligned} \tag{7}$$

with the extended Hamiltonian function,

$$\begin{aligned}H_{\text{ext}}\equiv\sum_{i=1}^{N}\Bigg[&\frac{1}{2m_i}(p_{x_i}^2+p_{y_i}^2+p_{z_i}^2)+\frac{1}{2m_i}(\Lambda_{x_i}^2+\Lambda_{y_i}^2+\Lambda_{z_i}^2)\\&+\frac{\hbar^2}{8m_i}(\rho_{x_i}^{-2}+\rho_{y_i}^{-2}+\rho_{z_i}^{-2})\Bigg]+\sum_{i<j}^{N}\langle V_{ij}(x_{ij},y_{ij},z_{ij})\rangle.\end{aligned} \tag{8}$$

Note that the mass and $\hbar$ have been retrieved here and they will be hereafter explicitly shown. $\{q_{\alpha_i},p_{\alpha_i}\}$ and $\{\rho_{\alpha_i},\Lambda_{\alpha_i}\}$ can be regarded as conjugate coordinate and momentum pairs. The $6N$-dimensional phase space is now extended to

Downloaded 14 Sep 2009 to 171.64.125.187. Redistribution subject to AIP license or copyright; see http://jcp.aip.org/jcp/copyright.jsp

京都大学 KYOTO UNIVERSITY
A Self-archived copy in
Kyoto University Research Information Repository
https://repository.kulib.kyoto-u.ac.jp
京都大学学術情報リポジトリ KURENAI 紅 Kyoto University Research Information Repository

the $12N$-dimensional phase space by the time-dependent Hartree approximation and variational principle. The system dynamics can be described with the potential concept in this extended Hamiltonian; the first two parts in Eq. (8) represent the kinetic energy, while the remaining two parts define the extended potential V_{ext}.

The potential $V_{ij}(x_{ij}, y_{ij}, z_{ij})$ can be expanded around $\langle x_i\rangle$, $\langle y_i\rangle$, and $\langle z_i\rangle$ as

$$\begin{aligned}\sum_{i<j}^{N} V_{ij}(x_{ij},y_{ij},z_{ij}) &= \sum_{i<j}^{N} V_{ij}(\langle x_{ij}\rangle,\langle y_{ij}\rangle,\langle z_{ij}\rangle) + \sum_{i=1}^{N} \left.\frac{\partial V_{ij}}{\partial x_i}\right|\Delta x_i + \sum_{i=1}^{N} \left.\frac{\partial V_{ij}}{\partial y_i}\right|\Delta y_i + \sum_{i=1}^{N} \left.\frac{\partial V_{ij}}{\partial z_i}\right|\Delta z_i + \sum_{i\neq j}^{N} \left.\frac{\partial^2 V_{ij}}{\partial x_i\,\partial y_j}\right|\Delta x_i\Delta y_j \\ &+ \sum_{i\neq j}^{N} \left.\frac{\partial^2 V_{ij}}{\partial y_i\,\partial z_j}\right|\Delta y_i\Delta z_j + \sum_{i\neq j}^{N} \left.\frac{\partial^2 V_{ij}}{\partial z_i\,\partial x_j}\right|\Delta z_i\Delta x_j + \sum_{i<j}^{N} \left.\frac{\partial^2 V_{ij}}{\partial x_i\,\partial x_j}\right|\Delta x_i\Delta x_j + \sum_{i<j}^{N} \left.\frac{\partial^2 V_{ij}}{\partial y_i\,\partial y_j}\right|\Delta y_i\Delta y_j \\ &+ \sum_{i<j}^{N} \left.\frac{\partial^2 V_{ij}}{\partial z_i\,\partial z_j}\right|\Delta z_i\Delta z_j + \sum_{i<j}^{N} \frac{1}{2} \left.\frac{\partial^2 V_{ij}}{\partial x_i^2}\right|\{(\Delta x_i)^2 + (\Delta x_j)^2\} + \sum_{i<j}^{N} \frac{1}{2} \left.\frac{\partial^2 V_{ij}}{\partial y_i^2}\right|\{(\Delta y_i)^2 + (\Delta y_j)^2\} \\ &+ \sum_{i<j}^{N} \frac{1}{2} \left.\frac{\partial^2 V_{ij}}{\partial z_i^2}\right|\{(\Delta z_i)^2 + (\Delta z_j)^2\} + \cdots, \end{aligned} \tag{9}$$

where $\Delta x_i = x_i - \langle x_i\rangle$, $\Delta y_i = y_i - \langle y_i\rangle$, and $\Delta z_i = z_i - \langle z_i\rangle$. All the differential coefficients should be calculated at $x_i = \langle x_i\rangle$, $y_i = \langle y_i\rangle$, and $z_i = \langle z_i\rangle$. Since Eq. (2) leads to $\langle \alpha_i\rangle = q_{\alpha_i}$, $\langle (\Delta\alpha_i)^2\rangle = \rho_{\alpha_i}^2$, and $\langle (\Delta\alpha_i)^4\rangle = 3\rho_{\alpha_i}^4$ for $\alpha_i = x_i$, y_i, and z_i, we obtain

$$\begin{aligned}\sum_{i<j}^{N} \langle V_{ij}(x_{ij},y_{ij},z_{ij})\rangle &= \sum_{i<j}^{N} V_{ij}(q_{x_{ij}},q_{y_{ij}},q_{z_{ij}}) + \sum_{i<j}^{N} \frac{1}{2} \left.\frac{\partial^2 V_{ij}}{\partial x_i^2}\right|(\rho_{x_i}^2 + \rho_{x_j}^2) + \sum_{i<j}^{N} \frac{1}{2} \left.\frac{\partial^2 V_{ij}}{\partial y_i^2}\right|(\rho_{y_i}^2 + \rho_{y_j}^2) + \sum_{i<j}^{N} \frac{1}{2} \left.\frac{\partial^2 V_{ij}}{\partial z_i^2}\right|(\rho_{z_i}^2 + \rho_{z_j}^2) \\ &+ \sum_{i<j}^{N} \frac{1}{4} \left.\frac{\partial^4 V_{ij}}{\partial x_i^2\,\partial x_j^2}\right|\rho_{x_i}^2\rho_{x_j}^2 + \sum_{i<j}^{N} \frac{1}{4} \left.\frac{\partial^4 V_{ij}}{\partial y_i^2\,\partial y_j^2}\right|\rho_{y_i}^2\rho_{y_j}^2 + \sum_{i<j}^{N} \frac{1}{4} \left.\frac{\partial^4 V_{ij}}{\partial z_i^2\,\partial z_j^2}\right|\rho_{z_i}^2\rho_{z_j}^2 + \sum_{i\neq j}^{N} \frac{1}{4} \left.\frac{\partial^4 V_{ij}}{\partial x_i^2\,\partial y_j^2}\right|\rho_{x_i}^2\rho_{y_j}^2 \\ &+ \sum_{i\neq j}^{N} \frac{1}{4} \left.\frac{\partial^4 V_{ij}}{\partial y_i^2\,\partial z_j^2}\right|\rho_{y_i}^2\rho_{z_j}^2 + \sum_{i\neq j}^{N} \frac{1}{4} \left.\frac{\partial^4 V_{ij}}{\partial z_i^2\,\partial x_j^2}\right|\rho_{z_i}^2\rho_{x_j}^2 + \sum_{i<j}^{N} \frac{1}{4} \left.\frac{\partial^4 V_{ij}}{\partial x_i^2\,\partial y_i^2}\right|(\rho_{x_i}^2\rho_{y_i}^2 + \rho_{x_j}^2\rho_{y_j}^2) \\ &+ \sum_{i<j}^{N} \frac{1}{4} \left.\frac{\partial^4 V_{ij}}{\partial y_i^2\,\partial z_i^2}\right|(\rho_{y_i}^2\rho_{z_i}^2 + \rho_{y_j}^2\rho_{z_j}^2) + \sum_{i<j}^{N} \frac{1}{4} \left.\frac{\partial^4 V_{ij}}{\partial z_i^2\,\partial x_i^2}\right|(\rho_{z_i}^2\rho_{x_i}^2 + \rho_{z_j}^2\rho_{x_j}^2) + \sum_{i<j}^{N} \frac{1}{8} \left.\frac{\partial^4 V_{ij}}{\partial x_i^4}\right|(\rho_{x_i}^4 + \rho_{x_j}^4) \\ &+ \sum_{i<j}^{N} \frac{1}{8} \left.\frac{\partial^4 V_{ij}}{\partial y_i^4}\right|(\rho_{y_i}^4 + \rho_{y_j}^4) + \sum_{i<j}^{N} \frac{1}{8} \left.\frac{\partial^4 V_{ij}}{\partial z_i^4}\right|(\rho_{z_i}^4 + \rho_{z_j}^4) + \cdots. \end{aligned} \tag{10}$$

All the differential coefficients are now calculated at $x_i = q_{x_i}$, $y_i = q_{y_i}$, and $z_i = q_{z_i}$. The first term $\Sigma_{i<j}^{N} V_{ij}(q_{x_{ij}}, q_{y_{ij}}, q_{z_{ij}})$ corresponds to the original classical potential function. The above equation results in Eq. (2.10) of Ref. 23 once x_i, y_i, and z_i are replaced by $q_{3(i-1)+1}$, $q_{3(i-1)+2}$, and q_{3i}, respectively. The EOM to be solved are

$$\dot{q}_{\alpha_i} = \frac{p_{\alpha_i}}{m_i}, \quad \dot{p}_{\alpha_i} = -\frac{\partial \Sigma_{i<j}^{N} \langle V_{ij}(x_{ij},y_{ij},z_{ij})\rangle}{\partial q_{\alpha_i}}, \tag{11}$$

$$\dot{\rho}_{\alpha_i} = \frac{\Lambda_{\alpha_i}}{m_i}, \quad \dot{\Lambda}_{\alpha_i} = -\frac{\partial \Sigma_{i<j}^{N} \langle V_{ij}(x_{ij},y_{ij},z_{ij})\rangle}{\partial \rho_{\alpha_i}} + \frac{\hbar^2}{4m_i\rho_{\alpha_i}^3} \tag{12}$$

from Eq. (7). If the symmetric (spherical) Gaussian WP basis functions are assumed, i.e., $\rho_{\alpha_i} = \rho_i$ and $\Lambda_{\alpha_i} = \Lambda_i$, in Eqs. (2) and (3), we get

Downloaded 14 Sep 2009 to 171.64.125.187. Redistribution subject to AIP license or copyright; see http://jcp.aip.org/jcp/copyright.jsp

京都大学 KYOTO UNIVERSITY
A Self-archived copy in
Kyoto University Research Information Repository
https://repository.kulib.kyoto-u.ac.jp
京都大学学術情報リポジトリ KURENAI 紅 Kyoto University Research Information Repository

$$\sum_{i<j}^{N}\langle V_{ij}(x_{ij},y_{ij},z_{ij})\rangle_{\mathrm{sym}}=\sum_{i<j}^{N}V_{ij}(q_{x_{ij}},q_{y_{ij}},q_{z_{ij}})+\sum_{i<j}^{N}\frac{1}{2}\left[\left.\frac{\partial^2V_{ij}}{\partial x_i^2}\right|+\left.\frac{\partial^2V_{ij}}{\partial y_i^2}\right|+\left.\frac{\partial^2V_{ij}}{\partial z_i^2}\right|\right](\rho_i^2+\rho_j^2)+\sum_{i<j}^{N}\frac{1}{4}\left[\left.\frac{\partial^4V_{ij}}{\partial x_i^2\,\partial x_j^2}\right|+\left.\frac{\partial^4V_{ij}}{\partial y_i^2\,\partial y_j^2}\right|+\left.\frac{\partial^4V_{ij}}{\partial z_i^2\,\partial z_j^2}\right|\right]\rho_i^2\rho_j^2+\sum_{i\neq j}^{N}\frac{1}{4}\left[\left.\frac{\partial^4V_{ij}}{\partial x_i^2\,\partial y_j^2}\right|+\left.\frac{\partial^4V_{ij}}{\partial y_i^2\,\partial z_j^2}\right|+\left.\frac{\partial^4V_{ij}}{\partial z_i^2\,\partial x_j^2}\right|\right]\rho_i^2\rho_j^2+\sum_{i<j}^{N}\frac{1}{4}\left[\left.\frac{\partial^4V_{ij}}{\partial x_i^2\,\partial y_i^2}\right|+\left.\frac{\partial^4V_{ij}}{\partial y_i^2\,\partial z_i^2}\right|+\left.\frac{\partial^4V_{ij}}{\partial z_i^2\,\partial x_i^2}\right|\right](\rho_i^4+\rho_j^4)+\sum_{i<j}^{N}\frac{1}{8}\left[\left.\frac{\partial^4V_{ij}}{\partial x_i^4}\right|+\left.\frac{\partial^4V_{ij}}{\partial y_i^4}\right|+\left.\frac{\partial^4V_{ij}}{\partial z_i^4}\right|\right](\rho_i^4+\rho_j^4)+\cdots \tag{13}$$

instead of Eq. (10). In this symmetric approximation, the extended Hamiltonian shown in Eq. (8) leads to

$$H_{\mathrm{ext}}\equiv\sum_{i=1}^{N}\left[\frac{1}{2m_i}(p_{x_i}^2+p_{y_i}^2+p_{z_i}^2)+\frac{3\Lambda_i^2}{2m_i}+\frac{3\hbar^2}{8m_i\rho_i^2}\right]+\sum_{i<j}^{N}\langle V_{ij}(x_{ij},y_{ij},z_{ij})\rangle_{\mathrm{sym}}. \tag{14}$$

The EOMs which we have to solve finally become

$$\dot{q}_{\alpha_i}=\frac{p_{\alpha_i}}{m_i},\quad \dot{p}_{\alpha_i}=-\frac{\partial\Sigma_{i<j}^{N}\langle V_{ij}(x_{ij},y_{ij},z_{ij})\rangle_{\mathrm{sym}}}{\partial q_{\alpha_i}}, \tag{15}$$

$$\dot{\rho}_i=\frac{\Lambda_i}{m_i},\quad \dot{\Lambda}_i=-\frac{\partial\Sigma_{i<j}^{N}\langle V_{ij}(x_{ij},y_{ij},z_{ij})\rangle_{\mathrm{sym}}}{3\,\partial\rho_i}+\frac{\hbar^2}{4m_i\rho_i^3} \tag{16}$$

for $i=1,2,\ldots,N$.

III. SEMIQUANTUM LIQUID WATER MOLECULAR DYNAMICS

We will develop the 3D SQW MD simulation using the 3D SQTDH for a many body system. In the present SQW simulation, only hydrogen atoms are calculated as semiquantum particles, while the oxygen atoms are simulated as classical particles like in the ordinary FCW simulation.[6–13]

A. Classical potential functions

We define ith water molecule consisting of three interaction sites centered on the atomic nuclei by the four internal degrees of freedom: two O–H bond lengths, r_{i,OH_1} and r_{i,OH_2}, O–H–O bond angle, $\theta_{i,\angle\mathrm{HOH}}$, and intramolecular H1–H2 length, $r_{i,\mathrm{H}_1\mathrm{H}_2}$. The intramolecular potential for ith molecule can be written as

$$V_{\mathrm{intra}}=\sum_{i=1}^{N_{\mathrm{mol}}}\left[\frac{k_{\mathrm{OH}}}{2}\{(r_{i,\mathrm{OH}_1}-r_{\mathrm{OH}}^0)^2+(r_{i,\mathrm{OH}_2}-r_{\mathrm{OH}}^0)^2\}+\frac{k_{\angle\mathrm{HOH}}}{2}(\theta_{i,\angle\mathrm{HOH}}-\theta_{\angle\mathrm{HOH}}^0)^2+\frac{k_{\mathrm{HH}}}{2}(r_{i,\mathrm{H}_1\mathrm{H}_2}-r_{\mathrm{H}_1\mathrm{H}_2}^0)^2\right], \tag{17}$$

where N_{mol} indicates the number of water molecules. $k_{\mathrm{OH}}=1054.2$ kcal mol^{-1} Å^{-2} and $k_{\angle\mathrm{HOH}}=75.9$ kcal mol^{-1} Å^{-2} denote the harmonic coefficients for the stretching and bending modes, respectively. $r_{\mathrm{OH}}^0=1.0$ Å and $\theta_{\angle\mathrm{HOH}}^0=113.24°$ are the corresponding equilibrium length and angle, respectively. The last term, called the Urey–Bradley term, gives a coupling between the valence bond angle and the chemical bond length with the coefficient $k_{\mathrm{HH}}=79.8$ kcal mol^{-1} Å^{-2} and the equilibrium length $r_{\mathrm{H}_1\mathrm{H}_2}^0=2r_{\mathrm{OH}}^0\sin(\theta_{\angle\mathrm{HOH}}^0/2)$. The Urey–Bradley term adds effective anharmonicity to the potential and makes it possible to reproduce the ground state splittings of the symmetric and antisymmetric stretching modes of a water molecule. The above model corresponds to the flexible SPC(SPC/Fd) model of water developed by Dang and Pettitt[6] except for $\theta_{\angle\mathrm{HOH}}^0$.[7] The equilibrium angle value was adopted from Ref. 7 which reported that $\theta_{\angle\mathrm{HOH}}^0$ significantly affects the dielectric constant. We found that the present dielectric constant is still smaller than the experimental dielectric constant of water liquid because a dielectric constant is sensitive to the way in which the truncation of long-range forces is treated, as well as $\theta_{\angle\mathrm{HOH}}^0$. It is possible, however, to correct the dielectric value using the reaction field approximation with an effective dielectric constant.[38]

The intermolecular potential can be written as

$$V_{\mathrm{inter}}=\sum_{i<j}^{N_{\mathrm{O}}}4\epsilon\left\{\left(\frac{\sigma}{r_{\mathrm{O}_i,\mathrm{O}_j}}\right)^{12}-\left(\frac{\sigma}{r_{\mathrm{O}_i,\mathrm{O}_j}}\right)^{6}\right\}+\sum_{i<j}^{N_{\mathrm{O}},N_{\mathrm{H}}}\frac{q_iq_j}{r_{ij}}, \tag{18}$$

where r_{ij} indicates distance between atoms i and j. N_{O} and N_{H} are the numbers of oxygen and hydrogen atoms, respectively. We took into account the Lennard-Jones interaction only for the oxygen atoms. $\sigma=3.165$ Å and $\epsilon=0.1554$ kcal mol^{-1} are uniform Lennard-Jones parameters for the oxygen atoms. q_i denotes a partial charge on an atom i, 0.41 a.u. for a hydrogen atom and -0.82 a.u. for an oxygen atom.

The total classical potential function is given by $V_{\mathrm{classical}}=V_{\mathrm{intra}}+V_{\mathrm{inter}}$. The classical potential function corresponds to the first term in Eq. (13). We have implemented a smooth cutoff method introducing the smooth cutoff function to circumvent the problems:[39,40] A simple abrupt cutoff of the potential function around boundary induces instability of the

Downloaded 14 Sep 2009 to 171.64.125.187. Redistribution subject to AIP license or copyright; see http://jcp.aip.org/jcp/copyright.jsp

京都大学 KYOTO UNIVERSITY
A Self-archived copy in
Kyoto University Research Information Repository
https://repository.kulib.kyoto-u.ac.jp
京都大学学術情報リポジトリ KURENAI 紅 Kyoto University Research Information Repository

energy, and the atom-based cutoff causes a charge neutrality problem for molecular pairs in boundary region. The potential function around boundary with the cutoff function is not applied to the semiquantum potentials derived in Sec. III B since the boundary region is determined only by distance between two oxygen atoms which are classically simulated.

B. Extended semiquantum potential functions

In order to calculate the EOM shown in Eqs. (15) and (16), we have to derive the differential coefficients displayed in Eq. (13) for V_{intra} and V_{inter}. Since quantum effects should be significant only for the hydrogen atoms, we need to derive the differential coefficients only for them. We emphasize that, however, while the oxygen atoms follow the classical potential function shown in Sec. III A, their dynamics are also influenced by additional nonclassical forces from the semiquantum hydrogen atoms.

The potential terms which we have to extend to semiquantum ones are the following three parts: the stretching potential functions of kth water molecule,

$$V^k_{\text{stretch},ij} = \frac{k_{ij}}{2}(r_{k,ij} - r^0_{ij})^2, \tag{19}$$

with $k_{ij}=k_{\text{OH}}$ or k_{HH}, and the bending potential function of kth water molecule,

$$V^k_{\text{bending},ij} = \frac{k_{\angle\text{HOH}}}{2}(\theta_{k,\angle i\text{O}j} - \theta^0_{\angle\text{HOH}})^2, \tag{20}$$

and the intermolecular Coulomb potential function,

$$V_{\text{Coulomb},ij} = \frac{q_i q_j}{r_{ij}}, \tag{21}$$

where at least one of i and j should be a hydrogen atom. Substituting these potential functions into the differential coefficients of Eq. (13) as V_{ij}, we can derive the extended potential functions. The partial differential should be performed only by Cartesian coordinates of the hydrogen atoms since only the hydrogen atoms are semiquantumly simulated. Owing to the symmetric Gaussian WP basis functions, we found that the sum of the fourth-order differential coefficients in Eq. (13) vanishes for all the stretching functions. As a result, the extended stretching potential functions to the fourth order becomes

$$\frac{1}{2}\left[\left|\frac{\partial^2 V^k_{\text{stretch},ij}}{\partial x_i^2}\right| + \left|\frac{\partial^2 V^k_{\text{stretch},ij}}{\partial y_i^2}\right| + \left|\frac{\partial^2 V^k_{\text{stretch},ij}}{\partial z_i^2}\right|\right](\rho_i^2 + \rho_j^2) = k_{ij}\left(3 - \frac{2r^0_{ij}}{r_{k,ij}}\right)(\rho_i^2 + \rho_j^2). \tag{22}$$

Note that when j is an oxygen atom, ρ_j^2 should be removed from Eq. (22), and that i and j should be atoms of the same molecule.

We will take into account the semiquantum corrections for the bending potential function only to the second order, partly because the higher-order forms are too complicated to be embedded in the MD program. This is also rationalized by a physical reasoning that the tightness of the bending potential maintains a nearly harmonic single well shape. In contrast, the higher-order expansions are essential for potentials of the double-well structure. The extended bending potential function is thus derived as

$$\begin{aligned}&\frac{1}{2}\left[\left|\frac{\partial^2 V^k_{\text{bending},ij}}{\partial x_i^2}\right| + \left|\frac{\partial^2 V^k_{\text{bending},ij}}{\partial y_i^2}\right| + \left|\frac{\partial^2 V^k_{\text{bending},ij}}{\partial z_i^2}\right|\right]\rho_i^2 \\ &+ \frac{1}{2}\left[\left|\frac{\partial^2 V^k_{\text{bending},ij}}{\partial x_j^2}\right| + \left|\frac{\partial^2 V^k_{\text{bending},ij}}{\partial y_j^2}\right| + \left|\frac{\partial^2 V^k_{\text{bending},ij}}{\partial z_j^2}\right|\right]\rho_j^2 \\ &= k_{\angle\text{HOH}}(1 + (\theta_{k,\angle i\text{O}j} - \theta^0_{\angle\text{HOH}})\cot\theta_{k,\angle i\text{O}j}) \\ &\times\left(\frac{\rho_i^2}{r^2_{k,i\text{O}}} + \frac{\rho_j^2}{r^2_{k,\text{O}j}}\right),\end{aligned} \tag{23}$$

where i and j should be hydrogen atoms of the same molecule.

The fully extended intermolecular Coulomb potential function had been obtained to describe dynamics of plasma.[41] Its rigorous form including the classical contribution, the last term of Eq. (18), is given by

$$\sum_{i<j}^{N_{\text{O}}N_{\text{H}}} \frac{q_i q_j}{r_{ij}}\text{erf}\left(\frac{r_{ij}}{\sqrt{2(\rho_i^2 + \rho_j^2)}}\right), \tag{24}$$

where ρ_j^2 should be removed when j is an oxygen atom. Now the all extended potential functions have been obtained, making it possible to calculate the SQW dynamics and structure using EOMs (15) and (16).

IV. SIMULATION DETAILS

The SQW and FCW systems are composed of 432 water molecules and were simulated in a cubic simulation box with a periodic boundary condition. The number of particles and the cubic system volume $V=(23.6)^3$ Å^3 were kept constant through the simulation. The mass density is set to be 0.982 g/cm^3, which is from the constant pressure Monte Carlo study[42] on the rigid TIP3P water at 298 K, 1 atm. All integration of the EOM is performed by the velocity-Verlet method with the time step 0.1 fs.

Equilibration methods for SQW are not fully understood yet. While the quantum variables account for ZPE and tunneling, at the same time the extra dimensionality leads to an overcounting of states available to the system if the phase space averaging is performed over both the classical and semiquantum variables. Indeed, assuming a Boltzmann distribution and integrating over all the dimensions including the semiquantum degrees of freedom to calculate the average system energy lead to extra energy in addition to the ZPE.[36] However, we may reasonably postulate that the classical degrees of freedom satisfy the canonical distribution at equilibrium even when embedded in the semiquantum simulation. In addition, radial distribution functions (RDFs) and diffusion constants are almost independent of the temperature-constraining methods such as the velocity scaling, Berendsen

Downloaded 14 Sep 2009 to 171.64.125.187. Redistribution subject to AIP license or copyright; see http://jcp.aip.org/jcp/copyright.jsp

京都大学 KYOTO UNIVERSITY
A Self-archived copy in
Kyoto University Research Information Repository
https://repository.kulib.kyoto-u.ac.jp
京都大学学術情報リポジトリ KURENAI 紅 Kyoto University Research Information Repository

and Nosé–Hoover methods.[43] In the present cooling and equilibration runs, we made only the classical velocity degrees of freedom influenced by the heat baths, the velocity scaling thermostat, and Berendsen methods, with $T=298$ K and the relaxation time 400 fs. Other degrees of freedom are *freely* time evolved by EOMs (15) and (16). After the careful cooling and equilibration runs, the whole phase space reach the thermal equilibrium owing to *heat conduction* between the degrees of freedom controlled by the heat baths and the other degrees of freedom free from the heat baths. Finally, we carried out the constant NVE (microcanonical) simulation for 2 ns. The time step of 0.1 fs gives good total energy conservation; the average root-mean-square (rms) deviations of the total energies were 2.0×10^{-2} kcal/mol for SQW and 1.1×10^{-2} kcal/mol for FCW. Another criterion for the trajectory accuracy is the ratio of the rms fluctuation of the total energy over that of the total kinetic energy, for which we obtained 9.0×10^{-4} for SQW and 5.2×10^{-4} for FCW. The resultant kinetic temperatures were found to be 298.6 K with the rms fluctuation 5.7 K for SQW and 297.7 K with the rms fluctuation 5.5 K for FCW. All averaged values except for the results of frequency domain reported in Sec. V were obtained by the microcanonical simulation for the last 100 ps during 2 ns. The results of frequency domain were averaged with phase space calculated by the same microcanonical simulation, but from 100 to 160 ps.

The computational costs for SQW and FCW are almost comparative since the EOM representing the semiquantum hydrogen WP widths include only the auxiliary WP coordinates and momenta and the computational bottleneck is the evaluation of the pair interactions of molecules rather than the integration of EOM. For example, the ratio of the CPU time for the reported SQW MD simulation to that for the FCW MD simulation is 1.188. The SQW MD simulation is computationally more feasible than the CMD method: While the CMD method requires discretization points along the imaginary time path of each hydrogen atom,[16] the reported SQW MD simulation only needs a single pair of WP coordinate ρ_i and momentum Λ_i to describe an ith hydrogen atom.

V. RESULTS AND DISCUSSIONS

The upper figure of Fig. 1 displays the sum of the intramolecular (E_{intra}), intermolecular potential (E_{pe}), and kinetic (E_{ke}) energies, i.e., $E_{\text{cl}}=E_{\text{intra}}+E_{\text{pe}}+E_{\text{ke}}$, as a function of time. E_{cl} in SQW fluctuates in the multiscale times, from subpicoseconds to tens of picoseconds. This multi-time-scale fluctuation in E_{cl} never appears in FCW as is shown by the dashed line since we ran the microcanonical MD simulation also in FCW. The newly introduced degrees of freedom, ρ_i and Λ_i, behave just like an energy reservoir in SQW. As shown in the upper-middle figure of Fig. 1, the intramolecular energy is smaller in SQW than in FCW. This is explained by the fact that the energy is distributed not only to the intramolecular motions but also to the semiquantum motions in each water molecule as the semiquantum potential and kinetic energies, i.e., $E_{\rho_{\text{pe}}}$ and $E_{\rho_{\text{ke}}}$. On the other hand, the lower-middle figure of Fig. 1 demonstrates that the intermolecular potential energy is higher in SQW than in FCW. This is because including the semiquantum hydrogen atoms, the liquid water is less structured and becomes unstable, as will be discussed later. No important difference is found in the kinetic energy data displayed in the lower figure of Fig. 1, rationalizing the minor difference in the rms fluctuation amplitude as noted for the kinetic temperature.

The new energies introduced by SQTDH are shown as a function of time in Fig. 2. As shown in the upper figure, the total semiquantum energy E_ρ fluctuates in the multiscale times, from subpicoseconds to tens of picoseconds. E_ρ and E_{cl} in SQW are complementary to each other since the sum of the two energies is well conserved owing to the microcanonical simulation. The E_ρ's constituents, the semiquantum potential $E_{\rho_{\text{pe}}}$, and kinetic $E_{\rho_{\text{ke}}}$ energies are shown in the middle and lower figures, respectively. E_ρ consists mainly of $E_{\rho_{\text{pe}}}$, while $E_{\rho_{\text{pe}}}$ and $E_{\rho_{\text{ke}}}$ fluctuate quite similarly.

The RDFs were calculated using the standard definition,

$$g(r)=\frac{\langle n(r)\rangle_{\text{av}}}{4\pi r^2 dr n_0}, \tag{25}$$

where $\langle\cdots\rangle_{\text{av}}$ means averaging over both time and individual molecules, $n(r)$ represents the number of molecules between shells of radii r and $r+dr$, and n_0 is the number density of the whole system.[44] The RDF $g(r)$ reflects the average liquid structure around a central atom. The $g(r)$ function for an oxygen-oxygen pair is shown in the upper figure of Fig. 3. The first peak position and height are in harmony with the corresponding experimental and PIMC results.[16,18,45] In the case of SQW, the liquid becomes less structured as reflected by lowered peaks and raised valleys in the RDF. Moreover, the average distance between the oxygen atoms of two neighboring water molecules increases in SQW; the first peak shifts from 2.74 to 2.76 Å. This result indicates that the effective interoxygen attraction for two neighboring oxygen atoms is reduced by the additional excluded volume effect or repulsive force induced by the WP semiquantum hydrogen atoms. The decrease in the structure of the liquid owing to a quantum-mechanical effect was also observed in the earlier PIMC calculations.[14–16,18] The $g(r)$ function for an oxygen-hydrogen pair provides a signature of the degree of hydrogen bonding. As shown in the upper-middle figure of Fig. 3, the first peak in SQW decreases and shifts from 1.74 to 1.76 Å, suggesting that hydrogen bonds are weakened when the hydrogen atoms show the semiquantum behavior. An overstructured first solvation shell seems common through many classical SPC variants, partly because the hydrogen-bonding network is enhanced by the hydrogen charge more exposed due to the fixed partial charge approximation.[46] In the present RDF for an oxygen-hydrogen pair, the first peak becomes lower than the second peak in SQW, which is in accord with the experimental and PIMC results.[16,18,47] The FCW has excessive hydrogen bonding and its longer lifetime of the hydrogen bonds results in an anomalously stable hydrogen bond network. The lower-middle figure of Fig. 3

Downloaded 14 Sep 2009 to 171.64.125.187. Redistribution subject to AIP license or copyright; see http://jcp.aip.org/jcp/copyright.jsp

京都大学 KYOTO UNIVERSITY
A Self-archived copy in
Kyoto University Research Information Repository
https://repository.kulib.kyoto-u.ac.jp
京都大学学術情報リポジトリ KURENAI 紅 Kyoto University Research Information Repository

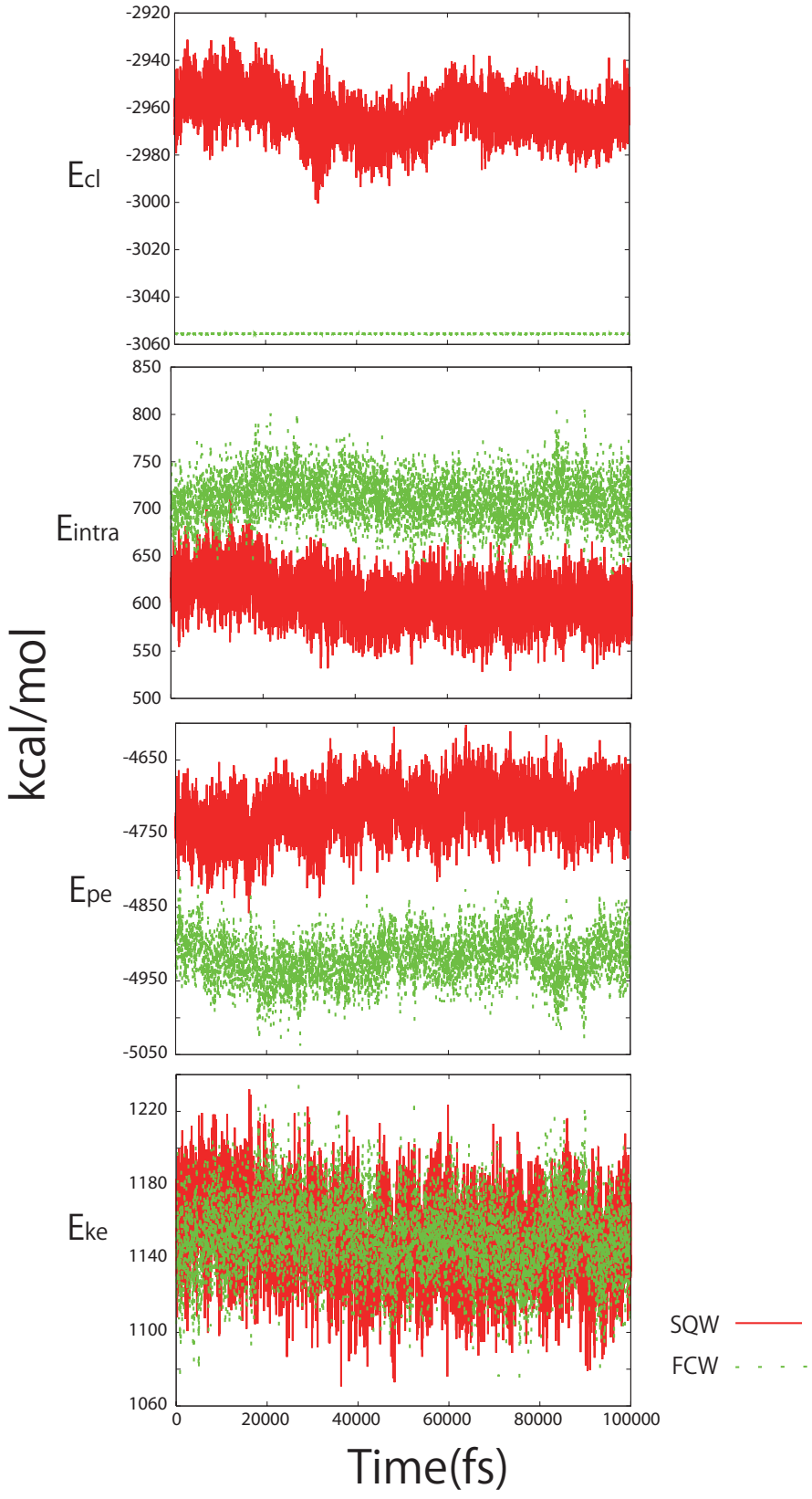

FIG. 1. Energies as a function of time. All the results from SQW are expressed by the solid lines, while the results from FCW are shown by the dashed lines. E_{cl} of SQW fluctuates not only in subpicoseconds but also in tens of picoseconds, while E_{cl} of FCW is well conserved (the upper figure). The newly introduced degrees of freedom behave just like an energy reservoir. The intramolecular energy E_{intra} is smaller in SQW than in FCW due to the additional energy distribution to the semiquantum degrees of freedom (the upper-middle figure), while the intermolecular potential energy E_{pe} is higher due to the poorer liquid structure (the lower-middle figure). The kinetic energy E_{ke} exhibits no significant difference between SQW and FCW except that the fluctuation is slightly larger in SQW (the lower figure).

Downloaded 14 Sep 2009 to 171.64.125.187. Redistribution subject to AIP license or copyright; see http://jcp.aip.org/jcp/copyright.jsp

京都大学 KYOTO UNIVERSITY
A Self-archived copy in
Kyoto University Research Information Repository
https://repository.kulib.kyoto-u.ac.jp
京都大学学術情報リポジトリ KURENAI 紅 Kyoto University Research Information Repository

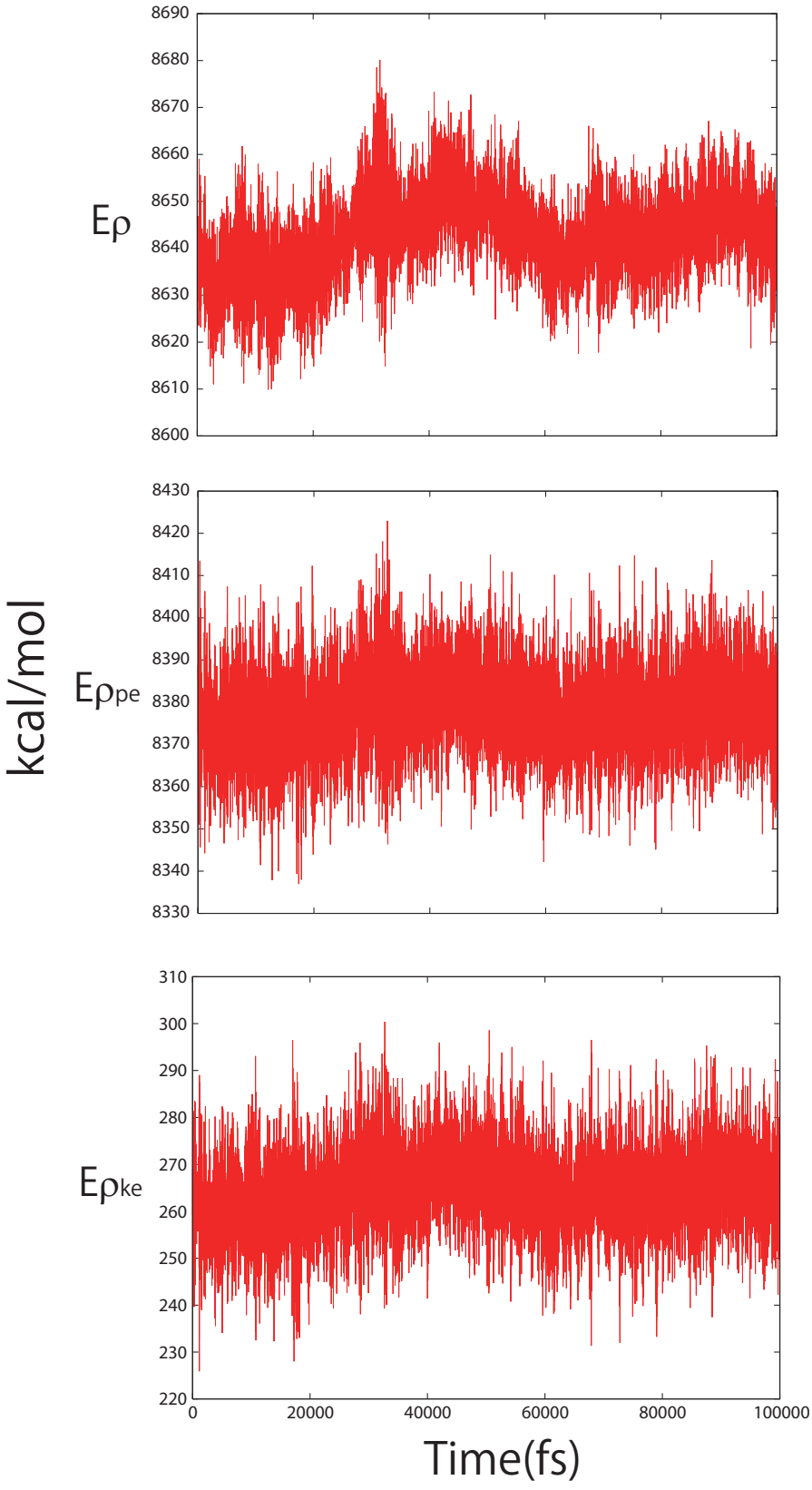

FIG. 2. New energies introduced by SQTDH. E_ρ is complementary to E_{cl} in SQW. E_ρ mainly consists of $E_{\rho_{\mathrm{pe}}}$. $E_{\rho_{\mathrm{pe}}}$ and $E_{\rho_{\mathrm{ke}}}$ fluctuate similarly and generate the multiscale modulation of E_ρ.

represents the $g(r)$ function for a hydrogen-hydrogen pair. The peak positions and heights are in harmony with the experimental and PIMC results.[16,18,45] The less structure of the intermolecular hydrogen atoms owing to the semiquantum effect was again observed.

The liquid structure can be further characterized by analyzing the relative orientation of water molecules. To this end, the two-dimensional (2D) distribution function,

Downloaded 14 Sep 2009 to 171.64.125.187. Redistribution subject to AIP license or copyright; see http://jcp.aip.org/jcp/copyright.jsp

京都大学 KYOTO UNIVERSITY
A Self-archived copy in
Kyoto University Research Information Repository
https://repository.kulib.kyoto-u.ac.jp
京都大学学術情報リポジトリ KURENAI 紅 Kyoto University Research Information Repository

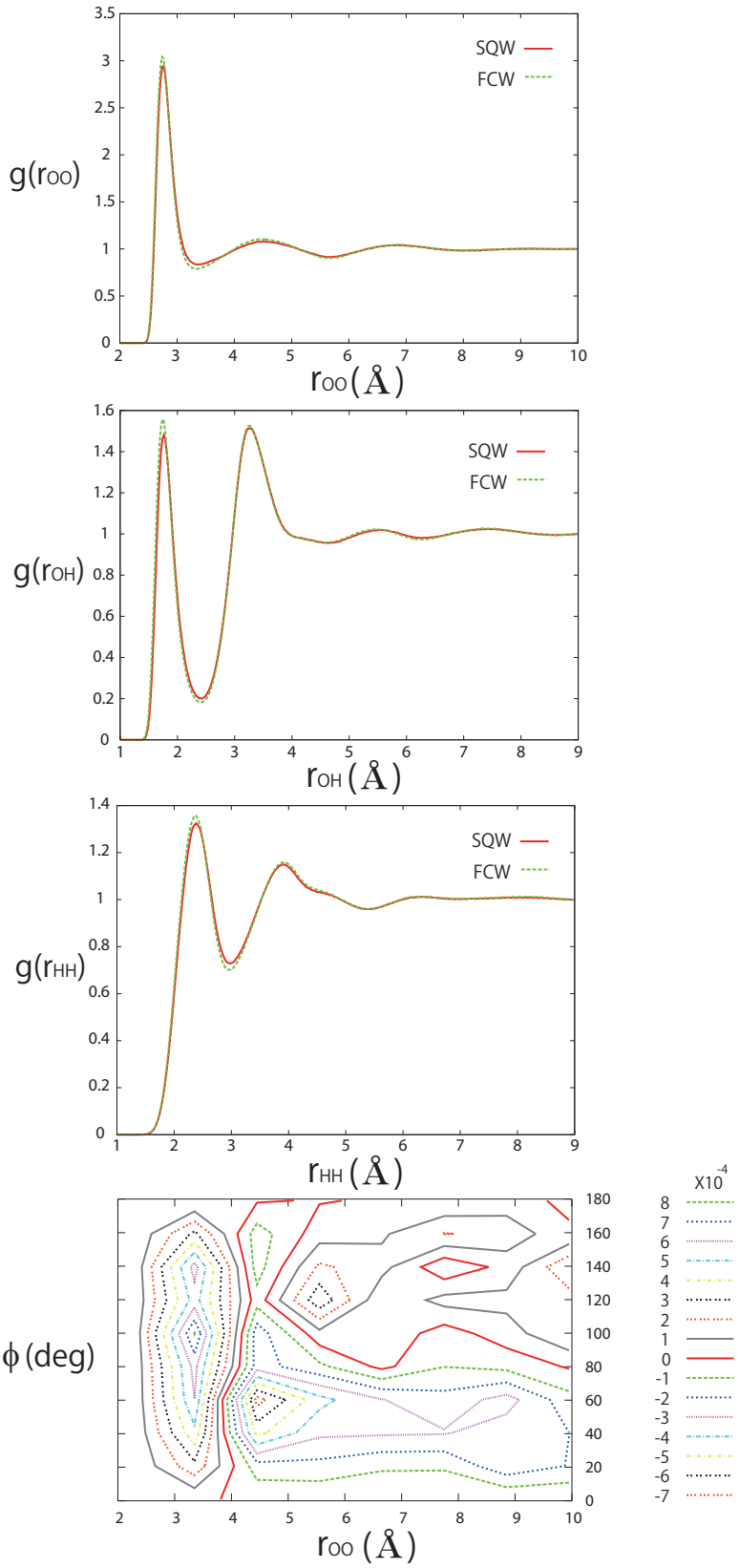

FIG. 3. RDFs for oxygen-oxygen atom pairs (the upper figure), for oxygen-hydrogen atom pairs (the upper-middle figure), and for hydrogen-hydrogen atom pairs (the lower-middle figure). The solid and dashed lines express the semiquantum and classical results, respectively. The liquid becomes less structured and the hydrogen bonds are weakened in SQW. The lower figure shows the difference between the semiquantum and classical 2D distribution functions of the radial distance for oxygen-oxygen atom pairs and the dipolar angle, Eq. (26). The structure rearrangement in SQW is quite systematic.

$$g(r_{OO},\phi)=\frac{\langle n(r_{OO},\phi)\rangle}{4\pi r^2 dr n_0}, \tag{26}$$

was calculated, where the radial coordinate r_{OO} is the distance between two oxygen atoms, and the angular coordinate ϕ is the angle formed by the dipole vectors of two water molecules(dipolar angle). The difference between the semiquantum and classical 2D distribution functions is shown in the lower figure of Fig. 3. We found that by semiquantizing the hydrogen atoms, the liquid structure rearranges not randomly nor uniformly but quite systematically. The broad positive peak is seen along 3.35 Å which indicates that the

Downloaded 14 Sep 2009 to 171.64.125.187. Redistribution subject to AIP license or copyright; see http://jcp.aip.org/jcp/copyright.jsp

京都大学 KYOTO UNIVERSITY
A Self-archived copy in
Kyoto University Research Information Repository
https://repository.kulib.kyoto-u.ac.jp
京都大学学術情報リポジトリ KURENAI 紅 Kyoto University Research Information Repository

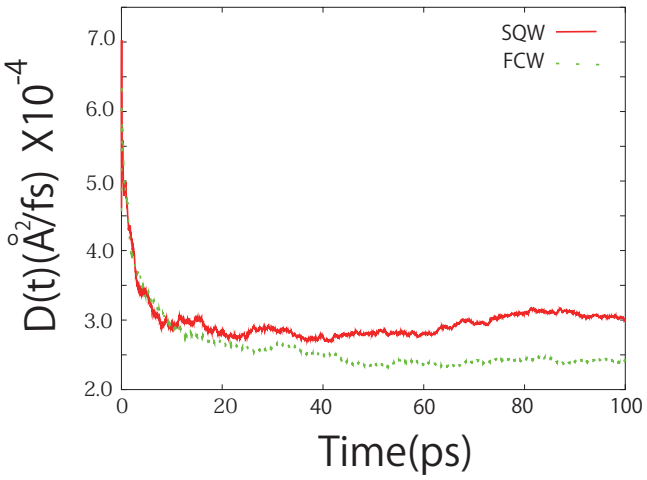

FIG. 4. Time-dependent self-diffusion. The solid and dashed lines denote the semiquantum and classical results, respectively. The converged values corresponds to the diffusion coefficients. The mobility of each water molecule increases in SQW.

first solvation shell waters became more distant from the central water molecule. Its two maxima appear around 100° and 140°, just avoiding 60° and 120°, which correspond to the angles between the central molecule and the well-structured first solvation shell molecules. The poor-structured first solvation molecules in FCW become poorer than the well-structured molecules when the semiquantum hydrogen atoms are introduced. On the other hand, beyond the first solvation shell, the well-structured water molecules are mainly rearranged, reflecting the negative peak around (4.5 Å, 60°) and the positive peak around (5.5 Å,120°). The former peak corresponds to the second solvation shell rearrangement.

Figure 4 shows the self-diffusion properties calculated from the slope of the mean-square displacement as a function of time,

$$D(t) = \frac{\langle |\mathbf{r}(t) - \mathbf{r}(0)|^2 \rangle_{\mathrm{mol}}}{6t}, \tag{27}$$

where $\mathbf{r}(t)$ denotes the position vector of the center of mass of a water molecule at time t and the brackets $\langle \cdots \rangle_{\mathrm{mol}}$ denote an average over individual water molecules.[44] No significant difference was found in the short-time self-diffusion properties. According to Einstein's relation, the diffusion coefficients are obtained by $\lim_{t\to\infty} D(t)$. We found that the semiquantum diffusion coefficient D_{sq} increases compared to the classical diffusion coefficient D_{cl}; $D_{\mathrm{sq}}=3.00\times10^{-4}$ Å^2/fs and $D_{\mathrm{cl}}=2.43\times10^{-4}$ Å^2/fs. Even though the average structure changes in each molecule shown in Fig. 3 seem small, the overall liquid structure changes are significant. As a result of the poor structure due to the WP semiquantum hydrogen atoms, the mobility of a water molecule increased. The increasing in the semiquantum diffusion constant can be partly related to the decreasing in the average OH bond length, i.e., 1.011 Å for SQW and 1.019 Å for FCW. The earlier classical MD study on liquid water reported that an increase in OH bond length leads to more structured liquid and stronger hydrogen bonds, and results in a smaller mobility of each water molecule.[7] We mention that, however, the shortened average OH bond length is caused not by changing the equilibrium OH bond length parameter r_{OH}^0 but by introducing the semiquantum hydrogen atoms in the present study. The additional excluded volume effect or repulsive force induced by the semiquantum hydrogen atoms could cause this decreasing in the average OH bond length. The reported quantum-mechanical effects evidently disrupting the hydrogen-bonding network also contribute to the accelerated water molecule diffusion. The present result is consistent with the previous reports that the quantum fluctuations introduced by the CMD simulation or the path-integral approaches tend to increase the diffusion in liquid,[16,18,20–22] although the origin of the present increased diffusion is different from such quantum fluctuations.

The product of the Beer–Lambert absorption coefficient $\alpha(\omega)$ and the frequency dependent index of refraction $I(\omega)$, is given by

$$\alpha(\omega)I(\omega) \sim \omega(1 - e^{-2\pi\beta\hbar\omega}) \int_{-\infty}^{\infty} d\tau e^{2\pi i\omega\tau} \langle \hat{\mathbf{d}}(0) \cdot \hat{\mathbf{d}}(t) \rangle, \tag{28}$$

where the integrand of the Fourier transform is the quantum dipole operator autocorrelation function. This quantum correlation function can be computed from the classical one by means of the identity,

$$\int_{-\infty}^{\infty} d\tau e^{2\pi i\omega\tau} \langle \hat{\mathbf{d}}(0) \cdot \hat{\mathbf{d}}(t) \rangle \sim \frac{\beta\hbar 2\pi\omega}{1 - e^{-\beta\hbar 2\pi\omega}} \int_{-\infty}^{\infty} d\tau e^{2\pi i\omega\tau} \langle \mathbf{d}(0) \cdot \mathbf{d}(t) \rangle, \tag{29}$$

which gives an approximation termed the *harmonic approximation*.[48,49] The integrand of the Fourier transform is now the classical dipole vector autocorrelation function. The standard deviation of $\mathbf{d}(0)\cdot\mathbf{d}(t)$ for SQW now becomes about 1.5 times larger than the standard deviation for FCW, reflecting the larger mobility of individual water molecules in SQW. The $\alpha(\omega)I(\omega)$ for various frequency ranges of SQW and FCW are shown in Fig. 5. In the lowest frequency range (0–1200 cm^{-1}) where the translational and rotational motions are reflected, no significant difference other than the intensity appears between SQW and FCW. The bending modes are seen in the frequency between 1200 and 2000 cm^{-1}. The two peaks appearing in FCW could be attributed to the angular and distortion motions due to the Urey–Bradley term, or to the hydrogen-bonded and free bending motions. In SQW, these two peaks are merged into the single peak around 1681 cm^{-1}. The semiquantum behavior of the hydrogen atoms can mix such two bending motions. Owing to the Urey–Bradley term, both the symmetric and antisymmetric OH stretching modes appear in the frequency between 3400 and 4000 cm^{-1}. The semiquantum peak set is redshifted compared to the classical peak set. This can be interpreted as the effect of the poor structurization due to the semiquantum hydrogen atoms; the OH stretching modes are *softened* since the liquid becomes less structured. In addition, the ZPE introduced by the semiquantum hydrogen atoms enhances the effect of anharmonic potentials, re-

Downloaded 14 Sep 2009 to 171.64.125.187. Redistribution subject to AIP license or copyright; see http://jcp.aip.org/jcp/copyright.jsp

京都大学 KYOTO UNIVERSITY
A Self-archived copy in
Kyoto University Research Information Repository
https://repository.kulib.kyoto-u.ac.jp
京都大学学術情報リポジトリ KURENAI 紅 Kyoto University Research Information Repository

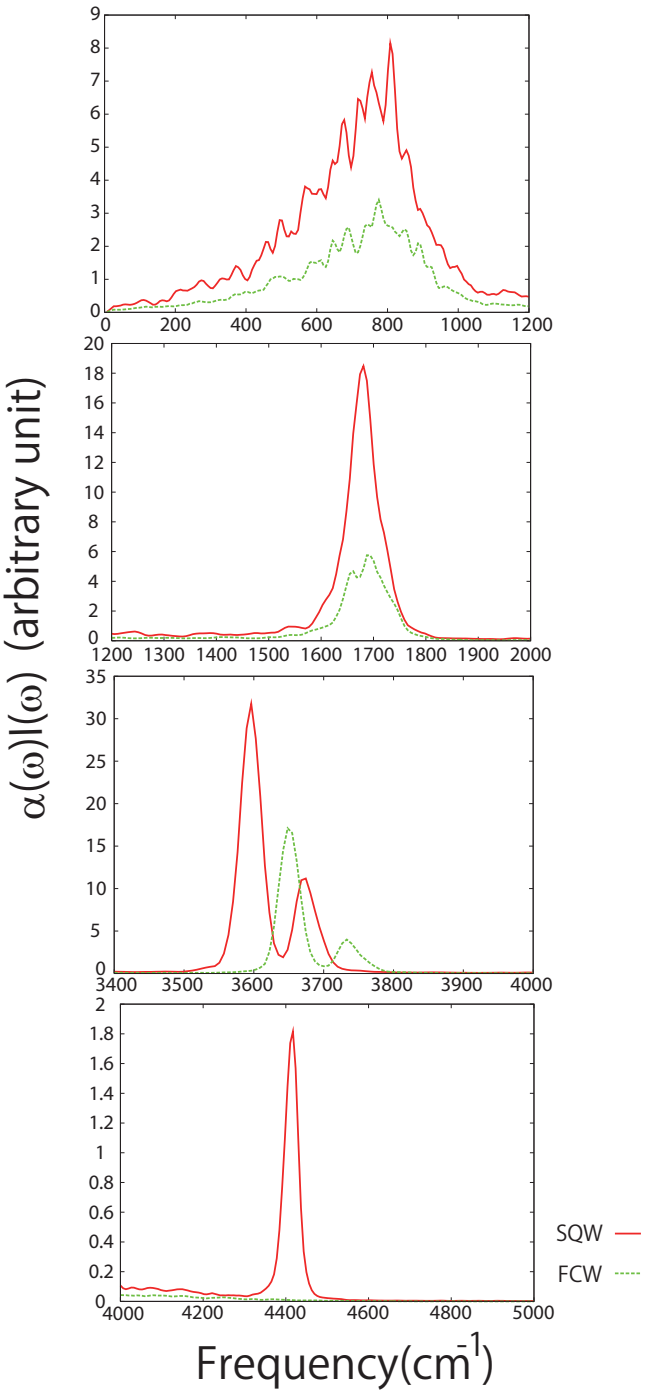

FIG. 5. $\alpha(\omega)I(\omega)$ for SQW and FCW shown by the solid and dashed lines, respectively. The split two bending peaks are merged into the one peak in SQW (the upper-middle figure). The semiquantum OH stretching modes are redshifted reflecting the softened poor structure due to the semiquantum hydrogen atoms and the potential anharmonicity picked up by the ZPE (the lower-middle figure). The significant peak originated from the quantum effect appears around 4400 cm^{-1} (the lower figure).

sulting in the redshifted OH stretching frequencies. Although the peak frequencies for OH stretching modes are slightly higher than the experimentally observed frequency,[50] it will be possible to adjust the present peaks to the experimental result by calibrating k_{OH} of Eq. (17). It should be mentioned that the roles of the semiquantum hydrogen atoms reported here are qualitatively unchanged even when such parametric constants are refitted. Moreover, as shown in the lower figure of Fig. 5, the semiquantum behaviors of the hydrogen atoms give a rise to the peak around 4400 cm^{-1}. The peak intensity is somewhat small, one-tenth of the other maximum peak intensity appearing around 1681 cm^{-1}. However, one could still identify this peak since there is only a few other significant peaks in the high frequency region, around 4400 cm^{-1}. The present peak could be an evidence of the quantum effects of hydrogen atoms since no peak appears around 4400 cm^{-1} in FCW.

Figure 6 demonstrates that this significant peak results from the energy exchange between the WP width and the sum of the symmetric OH stretching mode and the rotational motion of each water. In Fig. 5, the highest peak in the rotational frequency range is 808 cm^{-1}, while the peak position of the symmetric OH stretching mode appears at 3596 cm^{-1}. Thus, the sum of the two frequencies, 4404 cm^{-1}, is almost the same as the peak position around 4400 cm^{-1}. Actually, it is their power spectra which have the peak around 4400 cm^{-1}, as the upper and upper-middle figures of Fig. 6 show. The coupling of these two modes is also indicated by the peak appearing around the symmetric OH stretching frequency in the power spectrum of the rotational motion of a water molecular axis, while the peak around the antisymmetric OH stretching mode is much weaker (see the lower-middle figure of Fig. 6). The lowest figure of Fig. 6 displays the power spectrum of the time-dependent WP width ρ_i which shows the strong peak around 4400 cm^{-1}. The present frequency corresponds to the vibrational motion of the WP width representing the semiquantum hydrogen atoms. Since E_ρ and E_{cl} are complementary in SQW, energy of the frequency around 4400 cm^{-1} is exchanged between them. Only the coupling motion of the symmetric OH stretching mode and the rotational motion has a similar frequency, and can be resonant with the WP vibration. The WP motion has another peak around 3662 cm^{-1}, as the inset figure of Fig. 6 shows. However, this peak is covered by the OH stretching mode peaks and cannot be identified as a SQW-induced peak in Fig. 5.

We emphasize that the experimental IR and Raman signals of liquid water indeed show a small and yet unassigned peak at about 4000 cm^{-1} above the OH stretching peak at around 3500 cm^{-1}.[51] Our suggestion is also supported by the experimental results of D_2O;[51] the isotope effect less pronounces the corresponding peak above the OD stretching peak, indicating that the peak originates from quantum effects. Although the reported peak is in accord with the experimental results, both the intensity and the position are slightly overestimated. Because the peak reflects the energy exchange between the WP width and other water motions, the intensity could have been overenhanced in the present microcanonical simulation compared to a canonical condition. Also, since the WP vibrational motion is usually dependent on the intra- and intermolecular potentials more complicatedly than the OH stretching, the former peak deviation from the experimental results could be larger. In order to reproduce the experimental peak exactly, effective hydrogen mass might be needed instead of the normal hydrogen mass in Eq. (16). We note that since only hydrogen nuclei were calculated as semiquantum particles in the present SQW MD

Downloaded 14 Sep 2009 to 171.64.125.187. Redistribution subject to AIP license or copyright; see http://jcp.aip.org/jcp/copyright.jsp

京都大学 KYOTO UNIVERSITY
A Self-archived copy in
Kyoto University Research Information Repository
https://repository.kulib.kyoto-u.ac.jp
京都大学学術情報リポジトリ KURENAI 紅 Kyoto University Research Information Repository

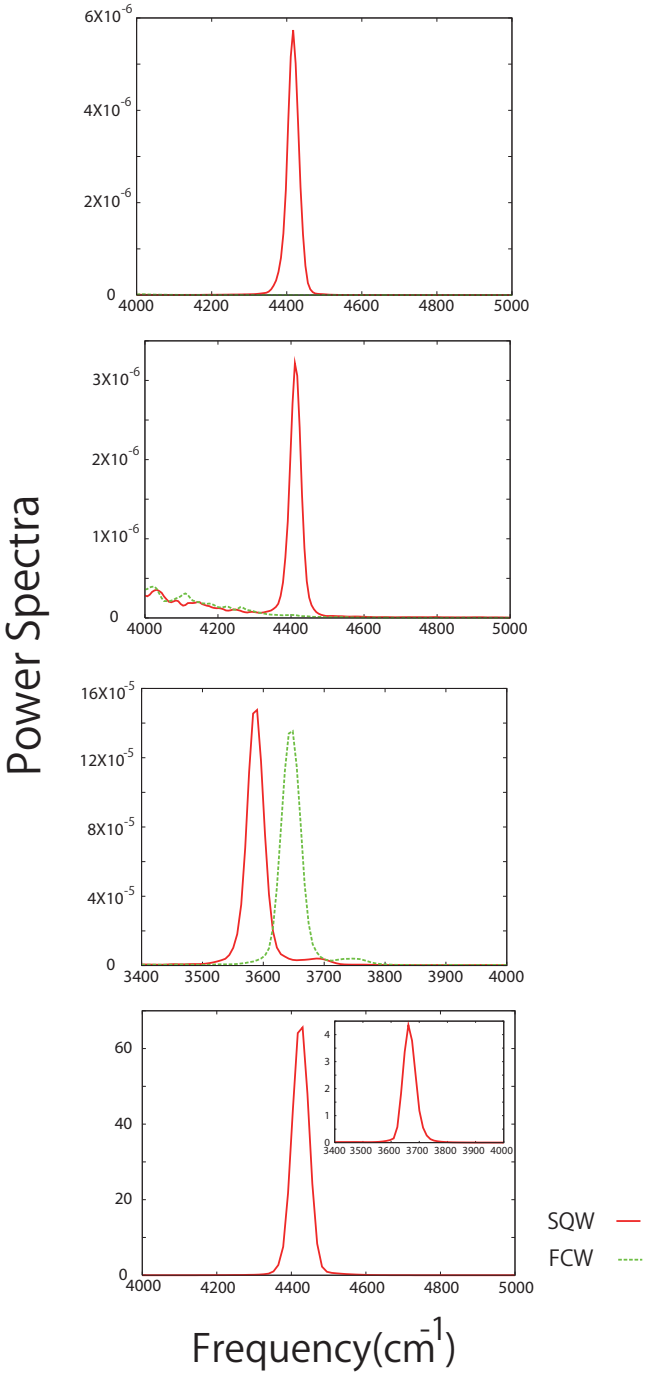

FIG. 6. Power spectra of the OH stretching mode (the upper figure) and of the rotational motion of a water molecule (the upper-middle and the lower-middle figures). The solid and dashed lines express the semiquantum and classical results, respectively. The lower-middle figure demonstrates that the rotational motion of a water molecule is coupled with the symmetric OH stretching mode. The power spectrum of the time-dependent WP width ρ_i in the lowest figure demonstrates that the vibrational motion of the WP width has the frequency of 4400 cm^{-1}. The energy exchange between the WP width dynamics and the coupling of the symmetric OH stretching mode and the rotational motion induces the significant peak around 4400 cm^{-1}.

simulation, the current peak is not due to fictitious electron mass as seen in the Car–Parrinello MD simulations.[52]

In Fig. 7, we provide the free energy schematic illustrations suggested from the reported SQW and FCW MD simulations. Semiquantum hydrogen atoms lead to less structured liquid water, and the free energy wells thus become greatly

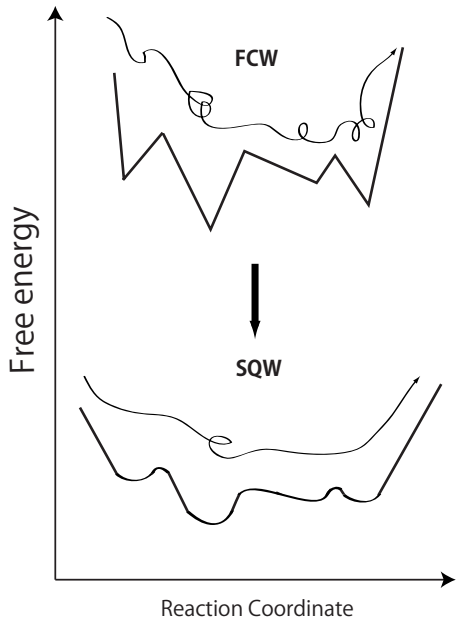

FIG. 7. Schematic illustration of the free energies in SQW and FCW. Our simulation results indicated that the free energy landscape should be smoothed in SQW compared to the classical one. The representative trajectories along a reaction coordinate are also shown for reference. A state in SQW moves more smoothly along the reaction coordinate due to the smoothed free energy landscape.

smooth as illustrated in Fig. 7. This was reflected by the increased mobility of a water molecule and partly by the OH stretching frequency redshift. This reduction in the free energy local structure shown in Fig. 7 is also interpreted as an effect of hydrogen ZPE introduced by SQTDH. We conclude that semiquantum hydrogen atoms play essential roles in determining the liquid free energy landscape, and, therefore, its structure and dynamics.

VI. CONCLUDING REMARKS

We have developed the SQW MD simulation method using the time-dependent Hartree approach. According to the 3D SQTDH approach, the classical intra- and intermolecular potential functions of hydrogen atoms in liquid water were extended to the potential functions describing the WP hydrogen atoms. Since the EOM representing the semiquantum hydrogen WP widths include only the auxiliary coordinates and momenta of the WP, many of the standard numerical tools of classical MD can be applied, facilitating its implementation and applications. The SQW was less structured and its hydrogen bonds were weakened, resulting in the increased mobility of a water molecule and the redshift of OH stretching frequency. The significant peak around 4400 cm^{-1} was induced by the energy exchange between the WP width motion and the coupling of the OH stretching mode and the rotational motion of a water molecule, indicating an evidence of the quantum effects of hydrogen atoms. Semiquantum hydrogen atoms make a liquid free energy landscape smoothed, and play essential roles in determining the structure and dynamics. The present SQW MD simulation is computationally feasible even in more complex systems, and can be applied to other important condensed phase simulations in biological

Downloaded 14 Sep 2009 to 171.64.125.187. Redistribution subject to AIP license or copyright; see http://jcp.aip.org/jcp/copyright.jsp

京都大学 KYOTO UNIVERSITY
A Self-archived copy in
Kyoto University Research Information Repository
https://repository.kulib.kyoto-u.ac.jp
京都大学学術情報リポジトリ KURENAI 紅 Kyoto University Research Information Repository

systems or chemical reactions in solution where a water molecule plays a significant role. Developing alternative equilibration method for SQW and introducing an asymmetric Gaussian WP basis function seem interesting open questions.

ACKNOWLEDGMENTS

K.H.D. would like to express sincere gratitude to Professor Y. Amou and Professor Y. Tominaga for showing the authors their unpublished experimental IR and Raman data on liquid water. K.H.D. is partially supported by the Grant-in-Aids for Scientific Research from Japan Society for the Promotion of Science (KAKENHI), Grant No. 20750010, and the research grant from the Showa Houkou Kai Foundation. K.A. acknowledges supports from KAKENHI in priority areas "Molecular Theory for Real Systems" (Grant No. 190296) and "Emergency of Highly Elaborated π-space and its Function" (Grant No. 20106017).

[1] N. Makri, Annu. Rev. Phys. Chem. **50**, 167 (1999).
[2] H. D. Meyer and G. A. Worth, Theor. Chem. Acc. **109**, 251 (2003).
[3] G. Mathias and D. Marx, Proc. Natl. Acad. Sci. U.S.A. **104**, 6980 (2007).
[4] C. Kandt, K. Gerwert, and J. Schlitter, Proteins: Struct., Funct., Bioinf. **58**, 528 (2005).
[5] J. M. J. Swanson, C. M. Maupin, H. N. Chen, M. K. Petersen, J. C. Xu, Y. J. Wu, and G. A. Voth, J. Phys. Chem. B **111**, 4300 (2007).
[6] L. X. Dang and B. M. Pettitt, J. Phys. Chem. **91**, 3349 (1987).
[7] Y. Wu, H. L. Tepper, and G. A. Voth, J. Chem. Phys. **124**, 024503 (2006).
[8] D. M. Ferguson, J. Comput. Chem. **16**, 501 (1995).
[9] I. G. Tironi, R. M. Brunne, and W. F. vanGunsteren, Chem. Phys. Lett. **250**, 19 (1996).
[10] T. Yagasaki and S. Saito, J. Chem. Phys. **128**, 154521 (2008).
[11] S. Saito and I. Ohmine, J. Chem. Phys. **102**, 3566 (1995).
[12] K. Toukan and A. Rahman, Phys. Rev. B **31**, 2643 (1985).
[13] S. Iuchi, A. Morita, and S. Kato, J. Phys. Chem. B **106**, 3466 (2002).
[14] R. A. Kuharski and P. J. Rossky, J. Chem. Phys. **82**, 5164 (1985).
[15] A. Wallqvist and B. J. Berne, Chem. Phys. Lett. **117**, 214 (1985).
[16] J. Lobaugh and G. A. Voth, J. Chem. Phys. **106**, 2400 (1997).
[17] T. D. Hone and G. A. Voth, J. Chem. Phys. **121**, 6412 (2004).
[18] F. Paesani, W. Zhang, D. A. Case, T. E. Cheatham, and G. A. Voth, J. Chem. Phys. **125**, 184507 (2006).
[19] L. Hernández de la Peña and P. G. Kusalik, J. Chem. Phys. **121**, 5992 (2004).
[20] L. Hernández de la Peña and P. G. Kusalik, J. Am. Chem. Soc. **127**, 5246 (2005).
[21] J. A. Poulsen, G. Nyman, and P. J. Rossky, Proc. Natl. Acad. Sci. U.S.A. **102**, 6709 (2005).
[22] T. F. Miller and D. E. Manolopoulos, J. Chem. Phys. **123**, 154504 (2005).
[23] K. Ando, J. Chem. Phys. **121**, 7136 (2004).
[24] K. Ando, J. Chem. Phys. **125**, 014104 (2006).
[25] H. J. Bakker and H. K. Nienhuys, Science **297**, 587 (2002).
[26] J. M. Headrick, E. G. Diken, R. S. Walters, N. I. Hammer, R. A. Christie, J. Cui, E. M. Myshakin, M. A. Duncan, M. A. Johnson, and K. D. Jordan, Science **308**, 1765 (2005).
[27] E. J. Heller, J. Chem. Phys. **62**, 1544 (1975).
[28] E. J. Heller, J. Chem. Phys. **64**, 63 (1976).
[29] M. H. Beck, A. Jackle, G. A. Worth, and H. D. Meyer, Phys. Rep. **324**, 1 (2000).
[30] I. Burghardt, M. Nest, and G. A. Worth, J. Chem. Phys. **119**, 5364 (2003).
[31] B. Jakob, P. G. Reinhard, C. Toepffer, and G. Zwicknagel, Phys. Rev. E **76**, 036406 (2007).
[32] M. Ben-Nun and T. J. Martinez, J. Chem. Phys. **108**, 7244 (1998).
[33] M. Ben-Nun and T. J. Martinez, J. Chem. Phys. **112**, 6113 (2000).
[34] E. Heatwole and O. V. Prezhdo, J. Chem. Phys. **121**, 10967 (2004).
[35] O. V. Prezhdo, Theor. Chem. Acc. **116**, 206 (2006).
[36] E. Heatwole and O. V. Prezhdo, J. Chem. Phys. **126**, 204108 (2007).
[37] Y. Shigeta, H. Miyachi, and K. Hirao, J. Chem. Phys. **125**, 244102 (2006).
[38] H. E. Alper and R. M. Levy, J. Chem. Phys. **91**, 1242 (1989).
[39] K. Ando, J. Phys. Chem. B **112**, 250 (2008).
[40] J. P. Bergsma, B. J. Gertner, K. R. Wilson, and J. T. Hynes, J. Chem. Phys. **86**, 1356 (1987).
[41] D. Klakow, C. Toepffer, and P. G. Reinhard, J. Chem. Phys. **101**, 10766 (1994).
[42] W. L. Jorgensen, J. Chandrasekhar, J. D. Madura, R. W. Impey, and M. L. Klein, J. Chem. Phys. **79**, 926 (1983).
[43] P. Mark and L. Nilsson, J. Comput. Chem. **23**, 1211 (2002).
[44] P. Allen and D. J. Tildesley, *Computer Simulations of Liquids* (Oxford Science, Oxford, 1987).
[45] J. M. Sorenson, G. Hura, R. M. Glaeser, and T. Head-Gordon, J. Chem. Phys. **113**, 9149 (2000).
[46] C. Kobayashi, K. Iwahashi, S. Saito, and I. Ohmine, J. Chem. Phys. **105**, 6358 (1996).
[47] A. K. Soper, Chem. Phys. **258**, 121 (2000).
[48] R. Iftimie and M. E. Tuckerman, J. Chem. Phys. **122**, 214508 (2005).
[49] H. Ahlborn, B. Space, and P. B. Moore, J. Chem. Phys. **112**, 8083 (2000).
[50] M. L. Cowan, B. D. Bruner, N. Huse, J. R. Dwyer, B. Chugh, E. T. J. Nibbering, T. Elsaesser, and R. J. D. Miller, Nature (London) **434**, 199 (2005).
[51] Y. Amou and Y. Tominaga (private communication).
[52] I. F. W. Kuo, C. J. Mundy, M. J. McGrath, and J. I. Siepmann, J. Chem. Theory Comput. **2**, 1274 (2006).

Downloaded 14 Sep 2009 to 171.64.125.187. Redistribution subject to AIP license or copyright; see http://jcp.aip.org/jcp/copyright.jsp